PROGRESS IN COLOR, COLORANTS AND COATINGS

available online @ www.pccc.icrc.ac.ir

Prog. Color Colorants Coat. 14 (2021), 161-178

Ministry of Science, Research and Technology
Institute for Color Science and Technology

Effect of Three Operating Variables on Degradation of Direct Blue 199 by TiO_2 Immobilized into a Polymer surface: Response Surface Methodology

O. Ounas[1,2*], B. Lekhlif[2], J. Jamal-Eddine[1]

[1.] Laboratory of Organic Synthesis, Extraction and Valorization, Department of Chemistry, Ain Chock Faculty of Sciences, Hassan II University, P.O. Box: 5366, Mâarif, Casablanca, Morocco.

[2.] Environmental Engineering Laboratory, Hassania School of Public Works, P. O. Box: 8108, Oasis, Casablanca, Marocco.

ARTICLE INFO

Article history:
Received: 21 Apr 2020
Final Revised: 07 Sept 2020
Accepted: 12 Sept 2020
Available online: 26 Oct 2020

Keywords:
Photocatalysis
TiO_2
Poly methyl methacrylate
Immobilization
Experiment design
Response surface methodology.

ABSTRACT

This work aims to study the photodegradation of Direct Blue 199 dye. The investigation was performed using titanium dioxide-based films immobilized on a polymethyl methacrylate (PMMA) polymer, by a promising low coast technique. The characterization of the films by X-ray diffractometry, fourier transform infrared spectroscopy, scanning electron microscopy, UV-Visible transmittance, and fluorescence spectroscopy revealed the deposition of 13.76% by mass of TiO_2 with excellent adhesion to the polymer surface. However, the evaluation of the influence of three parameters (pH, initial TiO_2 concentration, H_2O_2 concentration) on the efficiency of color removal in aqueous solution under UV irradiation on suspended semiconductors, have been performed using the response surface methodology based on experimental design. We therefore found the following optimum conditions: pH= 8, $[TiO_2]$ = 1369.29 $mg.L^{-1}$, $[H_2O_2]$ = 40 $mmol.L^{-1}$ which led to a discoloration efficiency of 85 %. The results were then used to evaluate the performance of the prepared photocatalyst films, which showed a strong capacity to absorb the dye due to the appearance of pores relative to the preparation procedure, in addition to their catalytic effect. The kinetic of decolorization under optimum conditions was well fitted to the pseudo-first-order kinetic model. Prog. Color Colorants Coat. 14 (2021), 161-178© Institute for Color Science and Technology.

1. Introduction

Organic contamination from different sources had become a significant concern due to the increasing environmental risk when they are discarded [1-6]. They have received considerable attention, especially those from chemical industries, which exhibit high toxicity, potential carcinogenic effects, and non-degradability. Thus, the efficient removal of such kinds of pollutants before discharging to the water bodies is becoming a significant problem. Due to the non-degradable nature and stability toward the light and/or oxidizing agents, dyes complicate the selection of a convenient removal method [1].

Several methods have been developed to treat the dye-containing effluents, including chemicals, physical, and biochemical processes, which did not ensure the complete mineralization of the organic pollutants from liquid waste. Among these methods, advanced oxidation processes are perhaps the best method for the removal of toxic pollutants [1, 2, 7-9].

One of the most effective methods of treating contaminated water is photocatalytic degradation [10]. TiO_2 is one of the widely used and studied photocatalyst for wastewater treatment. This is mainly due to its photo-stability, relatively low cost, low toxicity [11], and

*Corresponding author: o.ounas@gmail.com

high chemical stability [10]. The mechanism of using titanium dioxide directly in suspension is facing the technical challenge to separate the catalyst from the solution after treatment [12]. Thus, several recent studies focus on the immobilization of TiO_2 on different support [10, 12-17]. This immobilization can affect the photocatalytic performance, the surface, and the adsorption of the semiconductor. But it has the advantage of managing contaminated water continuously since it eliminates the need to separate catalyst particles once the water is treated [10, 18-20]. In this context, our previous study [12] on immobilizing TiO_2 onto the surface of PMMA polymer and its use as a photocatalyst, showed an excellent ability to degrade methylene blue as a model for organic pollutants with a degradation rate approaching 70%. But it was necessary to think of the optimization process to increase this rate and study the influence of common photocatalysis operational parameters. The parameters are commonly the initial concentration of the target compounds, degradation time, catalyst (type, dose, and characteristics), pH, and light source (temperature, nature, and irradiation intensity) [21, 22].

Traditionally, the most common practice when studying operational parameters is the traditional one-factor-at-a-time (OFAT) approach. It consists of finding the effect of one factor, which should vary systematically, while keeping other factors constant. Still, the result of this uni-variate analysis does not guarantee at all that the real optimum will be hit [21], because OFAT approach would be valid only if the factors to be optimized would be totally independent from each other [23]. Recent works tend towards chemometrics, and more specifically, Experimental Design (DoE). These processes study the effects of the factors influencing the experiment, and the relationship that can exist between them. The purpose of DoE is to obtain maximum information via minimum cost and time. Several studies in photocatalysis have chosen this vision of optimization [4, 20, 22, 24-35].

In the current study, we have chosen to use the statistical-based design of experiments (DoEs) methods such as response surface methodology (RSM). This method allowed finding and verifying the optimal conditions for Direct Blue 199 dye photodegradation. The photocatalyst was titanium dioxide-based films immobilized on the surface of a polymer prepared by a low coast method.

2. Experimental

2.1. Materials

Titanium dioxide was purchased from (MERCK Millipore) and used without further treatment. The reagents hydrogen peroxide, acetone, and polymethyl methacrylate polymer (average MW = 350.000 $g.mol^{-1}$) were purchased from Aldrich. The Direct Blue 199 dye ($C_{32}H_{18}CuN_9NaO_5S_2$, MW= 759.21 $g.mol^{-1}$) was supplied from "Mondial Chimie".

2.2. Preparation of the TiO_2/PMMA film photocatalysts

The preparation technique of the photocatalyst films (TiO_2/PMMA) used in this study, which was mentioned in our previous work [12] can be summarized as follows:

Magnetic stirring of a mixture of 1 g PMMA and 10 mL acetone for 24 h at 25 °C gave a solution that we took 1 mL and then spread on a glass plate, which was sprinkled previously with a thin layer of TiO_2 with the dimension of 10 × 8 cm, using a 1mm thick squeegee. The prepared film was left to dry for 60 min to evaporate the solvent and then washed with distilled water at 25°C several times to remove TiO_2 particle, which were not adhered to the polymer. The prepared film was then left 24h in distilled water to ensure the removal of any residual traces of the solvent and then put in the oven at 50°C for 24 hours before being used for the study of photodegradation.

2.3. Catalysts characterization

2.3.1. Zero-point charge (pH_{zpc})

A suspension with 0.5 g of the catalyst added to 25 mL of NaCl (0.1 mol L^{-1}) with an initial pH of 2, 4, 6, 8, 10, and 12 was stirred for 24 h then the final pH was measured. The pH_{pzc} is the point where the curve pH_{final} verses $pH_{initial}$ intersects the straight line corresponding to $pH_{initial} = pH_{initial}$ [36].

2.3.2. Morphological and structural characterization

A series of analyses were performed on the prepared films. Fourier transform infrared (FTIR) was carried out using an IRspirit spectrophotometer from Shimadzu, with the absorbance wavelength range between 400 to 4000 cm^{-1}. X-ray diffraction (XRD) patterns were recorded on a Bruker D8 Advance

diffractometer, using Cu Kα radiation (λ = 1.54184 Å) with 2θ in the range of 10-80. UV-Vis spectrophotometer (PerkinElmer instruments- Lambda 900) was used to measure the transmittance; the fraction of the luminous flux passing through a material. The Siemens SRS 3000 spectrophotometer (Rh tube, 200 mbar vacuum, 30s measurement for each line) with wavelength dispersive X-ray fluorescence was used to analyze the chemical composition (mass percentage in elements). The surface morphology and structure were examined by scanning electron microscopy (SEM) with a HIROX sh-4000, with an accelerated voltage of 15 kV, an emission current of 110 µA using the SED detection mode in high vacuum.

2.4. Photocatalytic degradation

The artificial irradiation unit used for the photodegradation reactions consists of a homemade wooden box (30 × 20 × 15 cm) equipped with a 9W UV-A lamp spare bulb, set 10 cm aside from the reactor (Figure 1).

As the first step, we studied the used lamp (Figure 2), which spectrum allowed us to show that the wavelength of UV emission is 364 nm, and transient, which demonstrate that the light takes about 1.5 minutes to reach 830 Lx, its maximum energy level. As the second step, we inserted fans in our reactor in order to avoid possible thermal damages caused by the weak infrared rays.

In the box mentioned above, and to study the optimal conditions, we placed a borosilicate glass batch reactor (250 mL capacity), where we put quantities of H_2O_2 and TiO_2 designated by the experimental design in a 200 mL solution of Direct Blue 199 of 50 $mg.L^{-1}$ concentrations at different pH and 20 °C. Afterward, a 5cm/5cm photocatalyst film was immersed in the reactor, as mentioned earlier, containing dye solution having the optimum conditions.

Before illumination, every solution was stirred in the dark for 60 min to reach the adsorption-desorption equilibrium between the catalyst and the dye solution. During the photocatalytic reaction, we took 3mL of the solution out of the beaker at a regular interval and the emission obtained in UV-Vis spectrometer characterized the reaction unit. The film photocatalytic activity was evaluated by absorbance measurement at the wavelength associated with Direct Blue 199 (607 nm) (Figure 3).

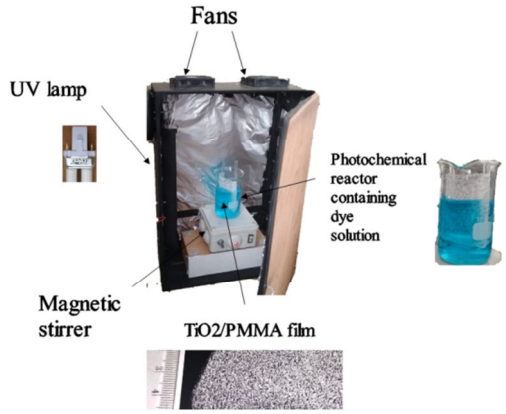

Figure 1: Schematic description of the homemade photoreactor used in photocatalytic degradation.

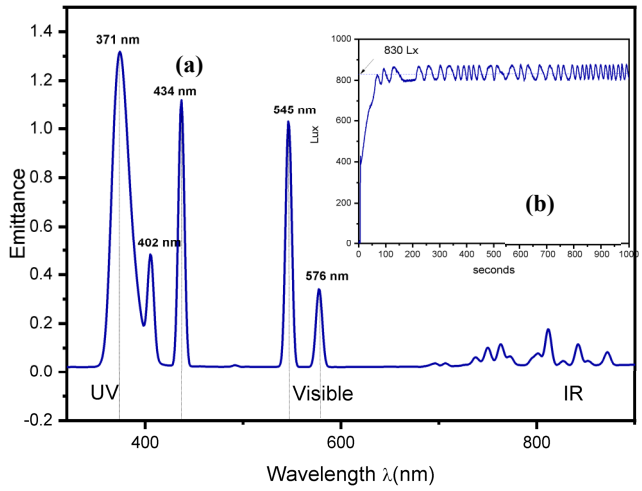

Figure 2: Emittance (a) and energy transient (b) of UV Lamp (365 nm).

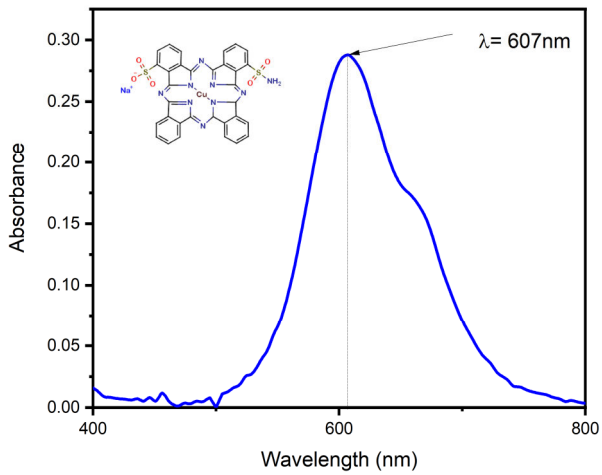

Figure 3: Absorbance spectrum of Direct Blue 199 dye and its molecular structure.

2.5. Design and statistical analysis of photocatalytic experiments

We found the optimal dye degradation conditions by using TiO_2 particles suspension before investigating the photocatalytic activity of the prepared films. For this, we used central composite experimental designs (CCD) to construct the response surface methodology (RSM) under various conditions. Such an approach makes it possible to study the process by modifying level factors employing a small number of experimental runs. The RSM objective is to optimize the response surface controlled by process parameters. RSM can estimate the linear, interaction, and quadratic effects of the parameters. Factors can be numerical and categorical, and the type of statistical factors can range from continuous to discrete [33]. Fundamental aspects related to DoE and RSM are widely presented in the scientific literature [21, 23, 37].

In this work, the effect of three independent variables, namely pH (X_1), catalyst mass (X_2), and H_2O_2 concentration (X_3), was investigated. Each variable (X_i) was converted to dimensionless code numbers to ease the statistical calculations and reduce error using the following equation (Eq. 1) [38]:

$$X_i = (X_i - X_0)/ \Delta X_i \quad (1)$$

where, X_0 is the value of X_i at the center point, and ΔXi is the step with maximum and minimum values of variable X_i. It should be noted that due to the importance of the reaction time factor, we omitted it in our study and chose to fix it in 1h30. Thus, the starting concentration of the dye was adjusted to 50 ppm. Also, the independent variables' ranges were selected through experiments obtained from the literature [39]. The CCD fractional factor model consists of three types of points: factorial, axial, and central. These points determine the total number of experiments (N), according to the relation (Eq. 2):

$$N=2^k +2k+nc \quad (2)$$

where k is the number of factors, 2^k is the runs at factorials points, 2k is the axial experiments, and nc is the central point replications (nc is often used to calculate the experimental error and the data reproducibility). As part of this work, 20 experiments were carried out, derived from the above equation: $N = 2^3 + (2\times3) + 6 = 20$.

The independent variables were then coded at low and high levels, −1 and +1, respectively. The axial points were located at (±α, 0, 0), (0, ±α, 0), and (0, 0, ±α), where α is the distance of the axial point from the center and makes the face-centered composite design. The α value was fixed at 1.362 (face-centered). The following second-order quadratic polynomial approximated the correlation between the response variable and the independent variable associated with the central composite matrix (Eq. 3);

$$R = \beta_0 + \Sigma\beta_i X_i + \Sigma\beta_{ij} X_i X_j + \Sigma\beta_{ii} X_i^2 + \varepsilon \quad (3)$$

where R is the response, β_0 is the constant coefficient, β_i, β_{ii}, and β_{ij} are the coefficients for the linear, quadratic, and interaction coefficient, respectively. X_i and X_j are the coded values, and ε is the residual term. The mathematical model fitting provides an equation to describe the response behavior in the selected DoE experimental domain. The least-square method was used for solving the equation and calculating the model coefficients. This method is multiple regression techniques for fitting a mathematical model to a set of experimental data producing the minimized sum of the squared differences between the actual and the predicted data. The fitting model goodness was evaluated by analysis of variance (ANOVA) (F-test, t-test, R^2, adjusted R^2, and lack-of-fit).

The optimum conditions for the variables were obtained by plotting the response surface in three dimensions (3D) and by contour plots through the determination of the coordinate axes. The software searches for a combination of factors that simultaneously satisfy the requirements placed on each

of the responses. The function called desirability (D) was established for determining the optimum performance levels for responses. Numerical optimization finds a point that maximizes the desirability function. This function is called objective, i.e. it goes from zero (low) outside the limits to one (maximum) to the goal. The Design-Expert software (Stat-Ease Inc., Minneapolis, USA), was used for data analysis, modeling, and evaluation of the statistical significance of the equations and optimization.

After applying the RSM, a confirmatory study stage was carried out under optimized conditions. When the confirmation results agree with the predictions, the developed model is said to be robust and insensitive to external noise.

3. Results and Discussion

3.1. Characterization analysis

Figure 4 shows the representative curve of the pH_{zpc} relative to the TiO_2. It defines the value where the surface charge of the oxide is neutral. Beyond this value (pH >6.5), the surface has a negative charge ($Ti\text{-}O^-$) and vice versa, i.e. when the pH is inferior to pH_{zpc} (pH <6.5) the surface is positive ($Ti\text{-}OH_2^+$). This characteristic affects the photocatalytic process because it determines the adsorption of entities on the catalyst surface.

The FTIR spectra of PMMA and TiO_2/PMMA thin films are shown in Figure 5. Vibration attribution and their locations are summarized in Table 1.

Table 1: FTIR bands assignment of PMMA, and TiO_2/PMMA films.

Vibration assignment	Wavenumber	Ref.
CH_2, C–O–CH_3	2992 cm^{-1}	[40]
CH	2951 cm^{-1}	[40]
Ester carbonyl group of PMMA	Sharp peak at 1727 cm^{-1}	[40]
C=O and –O–CH_3 groups of PMMA	1433 cm^{-1}	[40]
–CH_3 group	Small band at 1346 cm^{-1}	[40]
C–O (ester band) stretching vibration	Between 1260 cm^{-1} and 1146 cm^{-1}	[40]
Bending of C–H	At 978 cm^{-1} and 737 cm^{-1}	[40]
TiO_2 vibration	900cm^{-1}	[41]
Stretching mode of Ti-O	700cm^{-1}	[41]

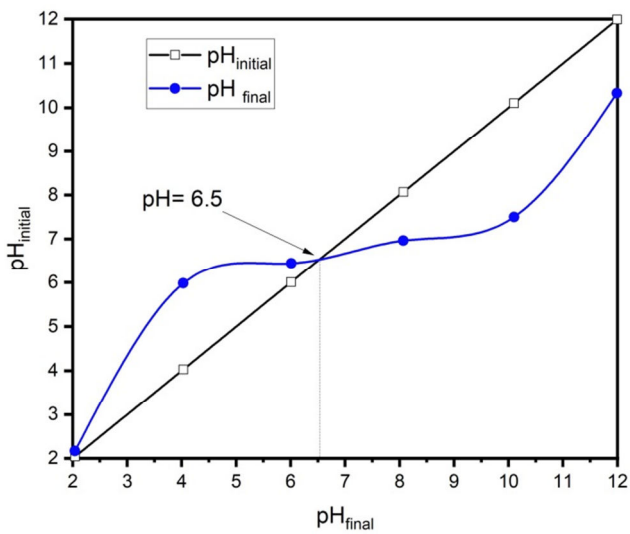

Figure 4: Point zero charge of TiO_2 photocatalyst.

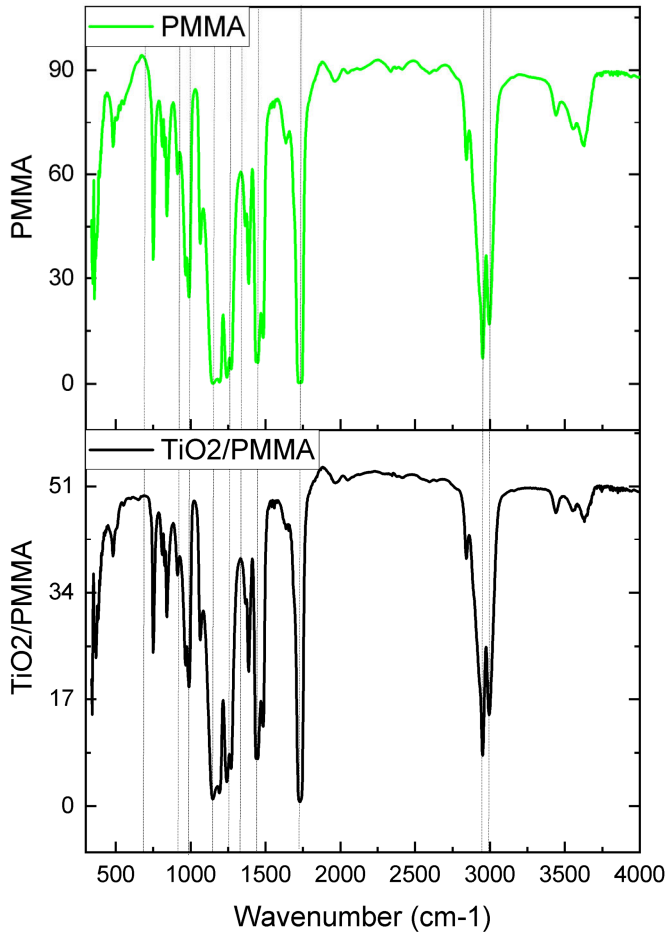

Figure 5: FTIR spectra of PMMA and TiO_2 /PMMA films.

In addition to the infrared spectrum, spectrophotometer allowed us to measure the thickness of the prepared films. The values obtained were 76.73 µm for the PMMA film and 92.17 µm for the TiO_2/PMMA film.

XRD investigated the crystallographic structure of the powder and films. Figure 6 reports the diffraction patterns of TiO_2 nanoparticle, PMMA film, and TiO_2/PMMA film. The XRD pattern of the PMMA film showed wide bands bonded to the amorphous structure of the polymer despite the appearance of peaks that are only due to the use of an adhesive tape to immobilize the film in the diffractometer. Instead, the TiO_2/PMMA film pattern evidenced, not only the presence of the PMMA matrix but also the Bragg peaks relative to the planes (101), (112), (105), (211), (116), (120) and (215) typical of the anatase crystal structure of the TiO_2 [42]. It means that the TiO_2 deposited on the PMMA film is in polycrystalline form, despite the low deposition temperature [43]. Other peaks present in the patterns are relatives to the adhesive used to immobilize the samples.

The TiO_2 XRD pattern was used to measure the average crystallite size by using the Scherrer's equation (Eq. 4) [44];

$$D= (k\times\lambda)/ (\beta\times\cos\theta) \quad (4)$$

where k is the Scherrer constant (0.9), λ is the wavelength of the X-ray irradiation and is equal to 0.154184 nm, β is the full width at half-maximum (FWHM), and θ is the Bragg angle in radian. The average crystallite size of the titanium oxides was 40.96 nm.

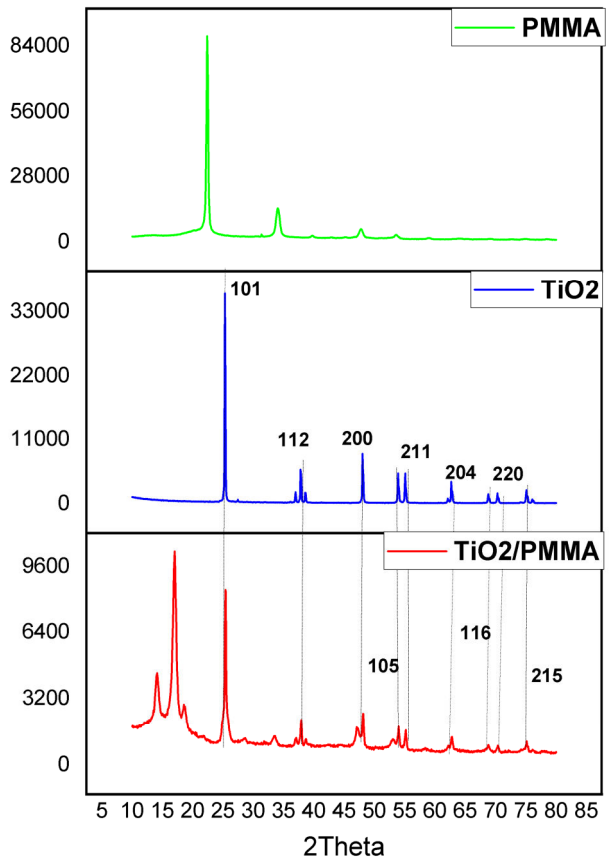

Figure 6: XRD pattern of TiO_2 powder, PMMA film and TiO_2/PMMA film.

Figure 7 shows the UV-Vis transmission spectra of the PMMA and TiO_2/PMMA films as a function of wavelength. PMMA films have high transparency compared to films loaded with TiO_2. The TiO_2 fixation into PMMA polymer reduces the film transmissions in different ranges; in UV re 60 to 35%, and in visible region from 78 to 45%, while infrared transparency decreases from 82 to 50%. This decrease in clarity is mainly attributed to the diffusion of light by the larger aggregates formed in TiO_2/PMMA films [45]. It confirms that TiO_2 is deposited very well on the polymer surface [46].

The PMMA films before and after immobilization were examined by scanning electron microscopy (SEM) to characterize the surface morphology, including the TiO_2 agglomerations and aggregations. The results are shown in Figure 8.

SEM images reveal the polymer surface's uniformity in the absence of the oxide (Figure 8 a). The incorporation of TiO_2 into the polymer matrix forms large agglomerates (Figure 8 b). These contain aggregates (Figure 8 c) whose size has been unlocked by processing images using Image J Software [47].

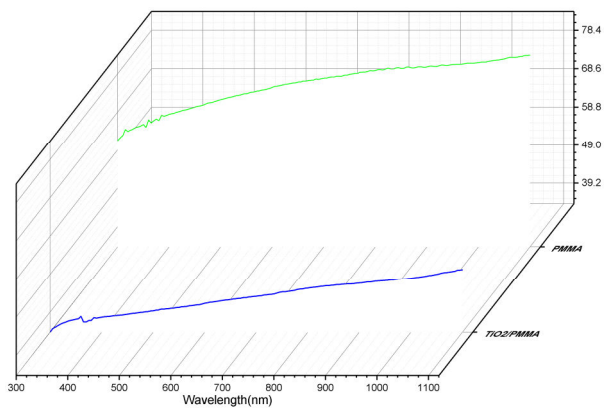

Figure 7: Transmittance spectra of PMMA film & TiO_2/PMMA film.

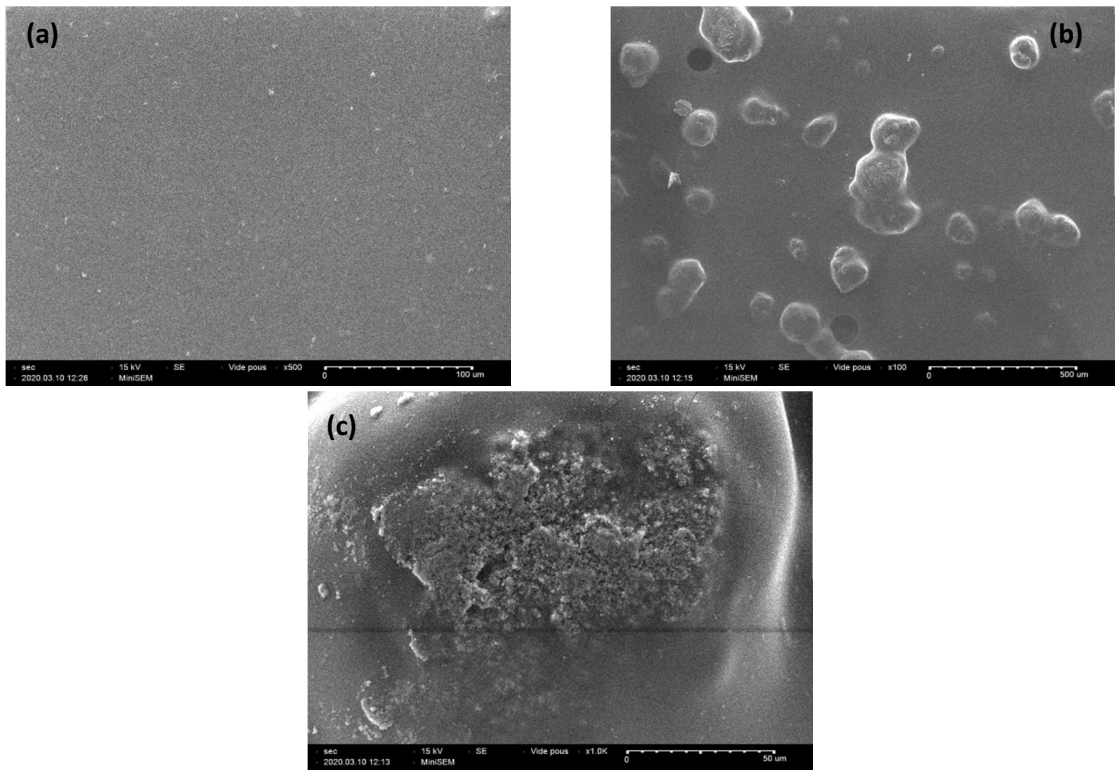

Figure 8: SEM images of (a) PMMA film and (b, c) TiO_2/PMMA film at different magnifications.

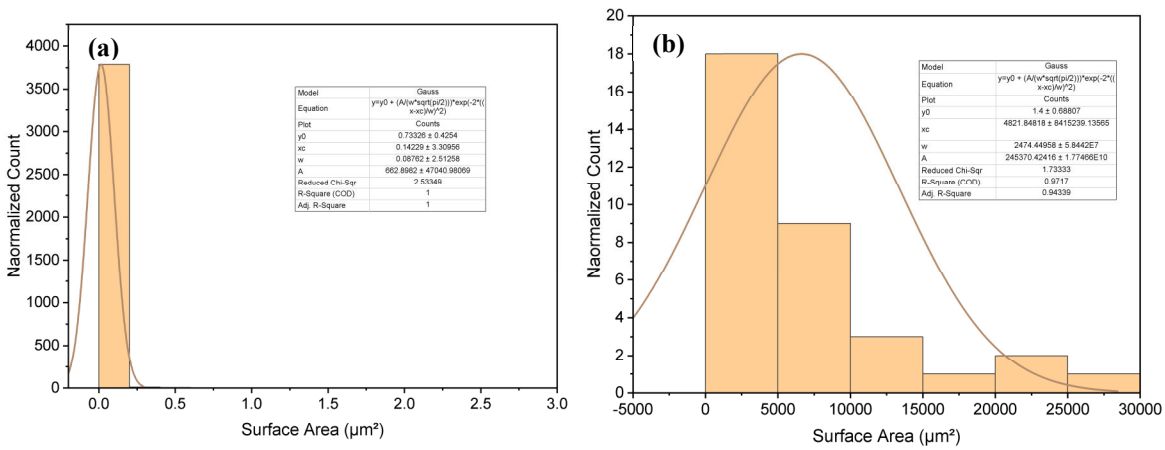

Figure 9: The area-equivalent number size distributions of TiO_2 agglomerates (a) & aggregates (b) determined by image analysis

The processing of the image at 500 µm (Figure 9 a) showed that the agglomerates have an average surface area of 4821.84 µm². From the image taken at 20 µm (Figure 9 b), we estimated that the average surface area of the aggregates forming the agglomerates was 0.142 µm², giving a diameter of 0.439µm.

The size and structure of the aggregates determine the reactivity of the materials. Therefore, a decrease in size leads to an increase in photocatalytic activity and vice versa. However, the aggregation is essential since it limits the problems associated with the release of nanoparticles into the environment [48]. SEM images confirm the effectiveness of TiO_2 deposition on the PMMA film, and subsequently, stable support was

obtained.

Finally, the analysis of the films prepared by X-ray fluorescence (Table 2) led to the conclusion that the preparation method allows the deposition of 13.76% by mass of TiO_2 on the PMMA polymer matrix.

3.2. Experimental design

3.2.1. Results of the model

The factors (input variables) to control the Direct Blue 199 dye degradation experiment were the solution pH, TiO_2 concentration ($mg.L^{-1}$) and H_2O_2 concentration ($mol.L^{-1}$). For modeling purposes, the factors were normalized to the same dimensionless scale (i.e. coded variables). The relationship between the actual (real) values of the factors and their coded levels are presented in Table 3.

A central composite design (CCD) type was applied to study the dye degradation process, as given in Table 4. The experimental design adopted involved 20 experimental trials. The performs 6-9-11-13-16-19 were used to test the reproducibility error. Table 4 summarizes the values of the observed response (discoloration efficiency determined for each test conducted under different pH, $[TiO_2]$, and $[H_2O_2]$ values.

Based on the collected data, an adjustment model was developed in terms of coded variables (A, B, and C) using the multiple regression method. It is given as follows (Eq. 5):

$$R=+19.06+ 5.76\ A+3.31B+8.02C+0.1008AB+1.48AC - 0.9036\ BC+3.46\ A^2 -1.70\ B^2 - 0.0689\ C^2 \quad (5)$$

where R is the expected discoloration efficiency (%), A, B, and C are coded factors; and $\alpha = 1.362$ is the axial point for the rotary design. The model developed (Eq. 5) represents a second-order polynomial equation with interaction terms, which has been statistically validated using analysis of variance (ANOVA).

The results of the ANOVA test are given in Table 5, showing a small p-value (less than 0.0001), indicating that the model is statistically significant.

The coefficient of determination (R^2) value suggests that the fitted model can explain 98% of the data variation. Also, the parity plot between the predicted and observed response (Figure 10) show that the multiple regression model is in good agreement with the observations. Thus, the parity plot (Figure 10) and the ANOVA results (Table 5) indicate the goodness of fit of the response surface models.

Table 2: Major elements in prepared films determined by X-RAY fluorescence (XRF).

Films	SiO_2	TiO_2	Al_2O_3	Fe_2O_3	MnO	MgO	CaO	Na_2O	K_2O	P_2O_5
PMMA	0	0	0	0	0.009	0	0.221	0.092	0	0.049
TiO_2/PMMA	0	13.768	0	0	0.009	0	0.15	0.069	0.183	0.126

Table 3: Design variables and their coded and actual values used for dye degradation experiments.

Design variables [factors]	Coded variables	Actual values of coded level				
		-α	+1	0	-1	+α
Solution pH	A	2.64	4	6	8	9.36
TiO_2 concentration	B	159.10	500	1000	1500	1840.90
H_2O_2 Concentration	C	-6.9	1	4.5	8	51.9

Table 4: Central composite design of the rotatable type used for experimentation.

Run	Design Variables						Response: Color removal efficiency
	Factor 1		Factor 2		Factor 3		
	pH	A	$[TiO_2]$ ($mg.L^{-1}$)	B	$[H_2O_2]$ ($mmol.L^{-1}$)	C	R (%)
1	6	0	1000	0	2.25	0	17.53
2	8	+1	1500	+1	0.5	-1	19.08
3	8	+1	500	-1	0.5	-1	12.01
4	*6*	*0*	*1000*	*0*	*51.9*	*+ α*	*32.57*
5	6	0	1840.9	+α	2.25	0	21.87
6	6	0	1000	0	2.25	0	17.75
7	8	+1	1500	+1	40	+1	37.88
8	6	0	159.10	- α	2.25	0	8.98
9	6	0	1000	0	2.25	0	19.51
10	4	-1	1500	+1	0.5	-1	11.63
11	6	0	1000	0	2.25	0	19.01
12	2.63	- α	1000	0	2.25	0	19.72
13	6	0	1000	0	2.25	0	20.01
14	4	-1	500	-1	0.5	-1	3.32
15	8	+1	500	-1	40	+1	32.78
16	6	0	1000	0	2.25	0	20.11
17	4	-1	1500	+1	40	+1	22.86
18	9.36	+ α	1000	0	2.25	0	40.26
19	6	0	1000	0	-6.9	- α	7.48
20	4	-1	500	-1	40	+1	19.81

Table 5: ANOVA test for the fitted model R (A; B; C) for predicting the discoloration efficiency.

Source	Sum of Squares	Degree of freedom	Mean Square	F-value	p-value	
Model	1738.39	9	193.15	68.97	< 0.0001	
A-pH	453.41	1	453.41	161.89	< 0.0001	
B-TiO_2	149.74	1	149.74	53.46	< 0.0001	
C-H_2O_2	877.69	1	877.69	313.38	< 0.0001	
AB	0.0813	1	0.0813	0.0290	0.8681	
AC	17.57	1	17.57	6.27	0.0312	**R^2 = 0.9841**
BC	6.53	1	6.53	2.33	0.1577	**Adjusted R^2 = 0.9699**
A^2	172.11	1	172.11	61.45	< 0.0001	**Predicted R^2 = 0.9005**
B^2	41.44	1	41.44	14.80	0.0032	**Significant Model**
C^2	0.0685	1	0.0685	0.0244	0.8789	
Residual	28.01	10	2.80			
Lack of Fit	21.75	5	4.35	3.47	0.0990	
Pure Error	6.26	5	1.25	-	-	
Cor Total	1766.40	19	-	-	-	

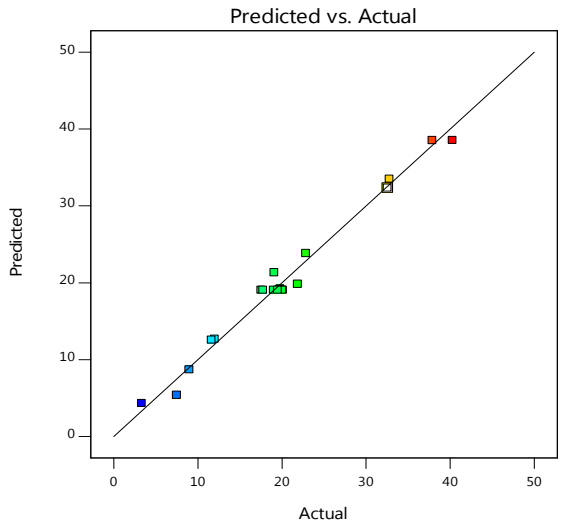

Figure 10: Parity plot between experimental observations and predictions for discoloration efficiency response.

Besides, the substitution technique made it possible to develop an empirical model, in terms of real factors, which can be written as follows (Eq. 6).

$$R=+13.04626-8.53994\ pH+0.021907\ TiO_2+1.58739\ H_2O_2+0.211684\ pH\times H_2O_2+0.863959\ pH^2-6.78270E-06\ TiO_2^2 \quad (6)$$

for $2.64 \leq pH \leq 9.36$; $159.1 \leq [TiO_2] \leq 1840.9$; $-6.9 \leq [H_2O_2] \leq 51.9$.

The model (Eq. 6) only contains significant terms, i.e. with p-values less than 0.0500.

3.2.2. Effect of operational variables

Using this model (Eq. 6), response areas and contour maps were plotted (Figures 11, 12 and 13), showing the mutual effects of the factors on the response (i.e. R, discoloration efficiency).

As shown in Figure 11, pH is the most significant factor influencing the evolution of the degradation process. The effect of TiO_2 concentration is weaker than that of the pH value. The removal efficiency (R) increases with the two elements increases. The effect of interaction between these two factors (pH and $[TiO_2]$) is not significant.

Figure 12 illustrates the combined effect of pH and $[H_2O_2]$ on the (R) response. As we can see, incrementing both factors (pH and $[H_2O_2]$) leads to an increase in discoloration efficiency. There is a small interaction effect between the two factors, since the effect of H_2O_2 concentration is more intense at higher pH (i.e., basic region). In contrast, the impact of pH is more evident at higher $[H_2O_2]$.

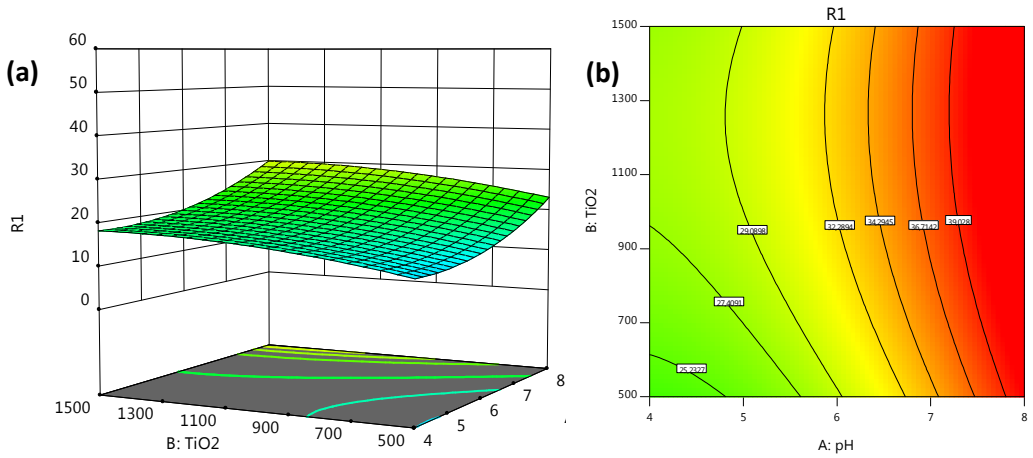

Figure 11: Response surface plot (a) and contour-line map (b) showing the combined effects of pH and $[TiO_2]$ factors on the discoloration efficiency R (%) under UV light irradiation, for the fixed level of $[H_2O_2]$= 51.9 mmol.L^{-1}.

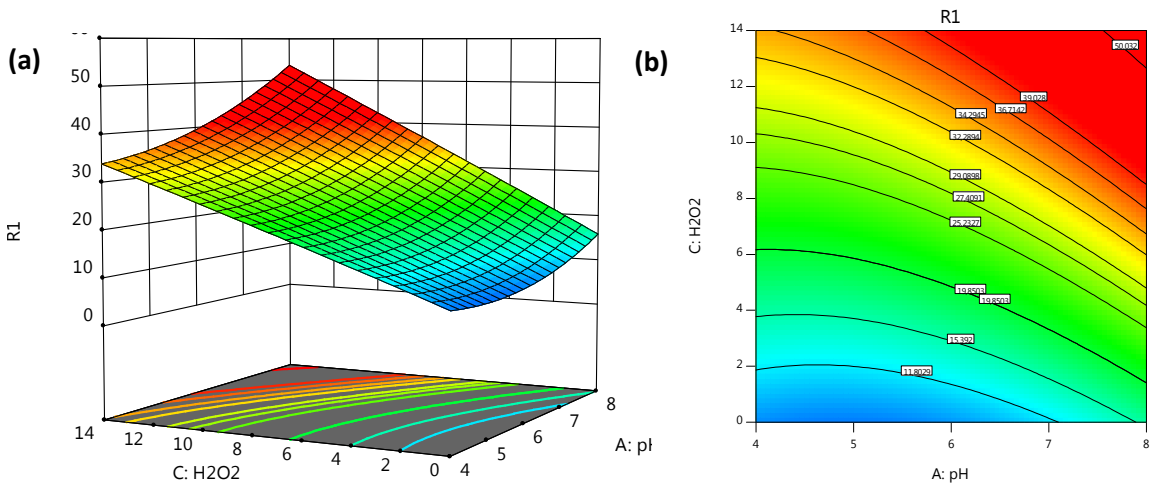

Figure 12: Response surface plot (a) and contour-line map (b) showing the combined effects of [H_2O_2] and pH factors on the discoloration efficiency R(%) under UV-light irradiation, for the fixed level of [TiO_2]=1000mg.L^{-1}.

As can be seen in Figures 11 and 12, moderate squared effects can be distinguished for the pH and [TiO_2] factors, while the squared result of [H_2O_2] is lower. From an economic point of view, working in mild conditions is recommended, hence the pH value in the range of 4-8 was chosen.

Moreover, the pH zero-point charge (pH_{zpc}) of the TiO_2 catalyst is a specific and essential effect. It allows the induction of the adsorption phenomena. Above and below the pH_{zpc} value, the catalyst is negatively or positively charged. Adsorption of cationic or anionic dyes, respectively, occurs with predilection. The pH_{zpc} of TiO_2 was around pH= 6.5. Direct Blue 199 dye has a positively charged structure; therefore, at basic pH values, the contaminant can be adsorbed effectively on the photocatalyst's surface. Consequently, we observed that the conversion was shallow at acidic pH compared to that produced at basic pH.

Figure 13 illustrates the effect between [TiO_2] and [H_2O_2] on the response (R). As can seen, the increase of both factors ([TiO_2] and [H_2O_2]) leads to the rise of the discoloration efficiency (R). The interaction effect between the two factors is minimal because by increasing the concentration of H_2O_2, the discoloration rate increases whatever the value of [TiO_2].

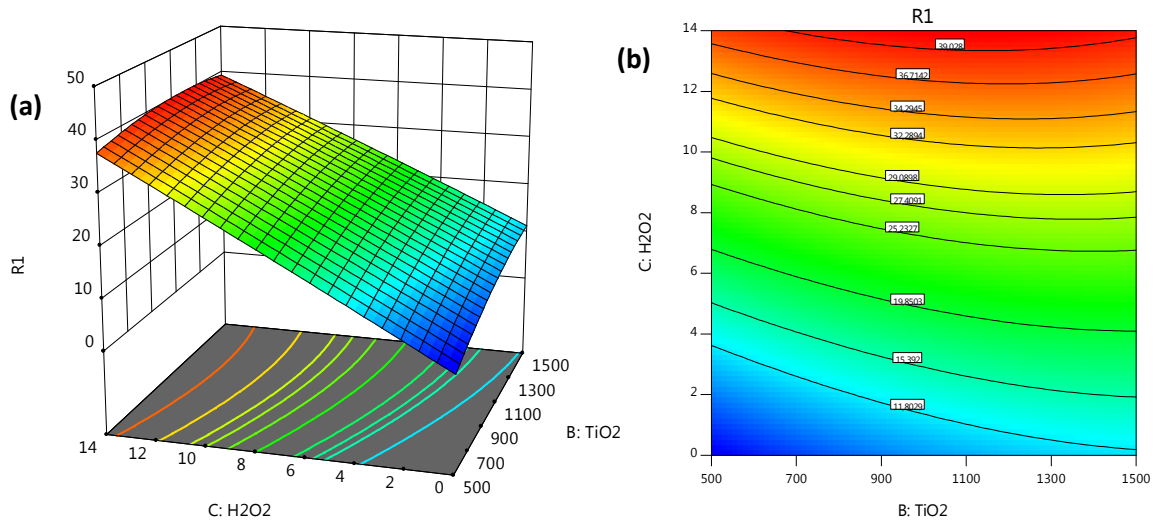

Figure 13: Response surface plot (a) and contour-line map (b) showing the combined effects of [H_2O_2] and [TiO_2] factors on the discoloration efficiency R(%) under UV-light irradiation, for the fixed level of pH=6.

3.2.3. Determination of optimal conditions for operational variables

After performing the response surface analysis, optimization was executed based on the desirability function to find the optimal conditions for Direct Blue 199 dye degradation. The software allows numerical optimization by locating the specific point that maximizes the desirability of a function. We selected the desired target by adjusting the weight or importance that could modify the goal's characteristics. The target fields for the answer have five options: none, maximum, minimum, target, and within range. Table 6 shows the optimization criteria of all the factors studied in correspondence with the percentage of degradation.

Based on the ANOVA test (Table 5), almost all the effects studied (pH, [TiO_2], and [H_2O_2]) were significant (p-value<0.0001), so these factors were classified as "in the range" with "importance 3". The mains goal is to obtain higher discoloration percentage; this is why "importance 5" was assigned to the supreme objective. The lower and upper bound values of all responses are taken from the CCD design levels.

The software optimized discoloration by using desirability functions (Figure 14), with all the parameters described above, and obtain pH=8, TiO_2 at 1369.28 $mg.L^{-1}$ and H_2O_2 at 40 $mmol.L^{-1}$, respectively.

3.2.4. Confirmatory study

Finally, for the validation, duplicate confirmatory experiments were conducted using the optimized parameters for the degradation of the Direct Blue 199 dye. The results are closely linked to the data from the optimization analysis.

It clearly appears in Figure 15 that the absorbance peak becomes almost smooth while the color of the solution becomes more and more transparent. The operating conditions found by the optimization give satisfactory results, and to obtain degradation close to 90%, it is enough to push the time of treatment (Figure 16).

Table 6: Optimization of the individual responses in order to obtain the overall desirability response (D).

Name	Goal	Lower Limit	Upper Limit	Importance
A: pH	is in range	4	8	3
B:TiO_2	is in range	500	1500	3
C:H_2O_2	is in range	1	8	3
R1	maximize	3.321	40.269	5

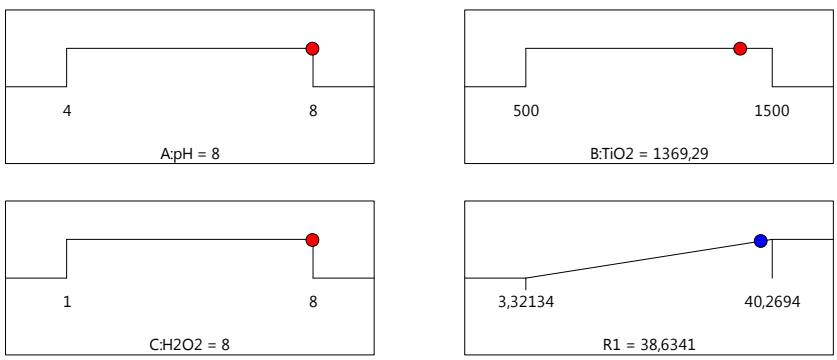

Figure 14: Desirability ramp for numerical optimization.

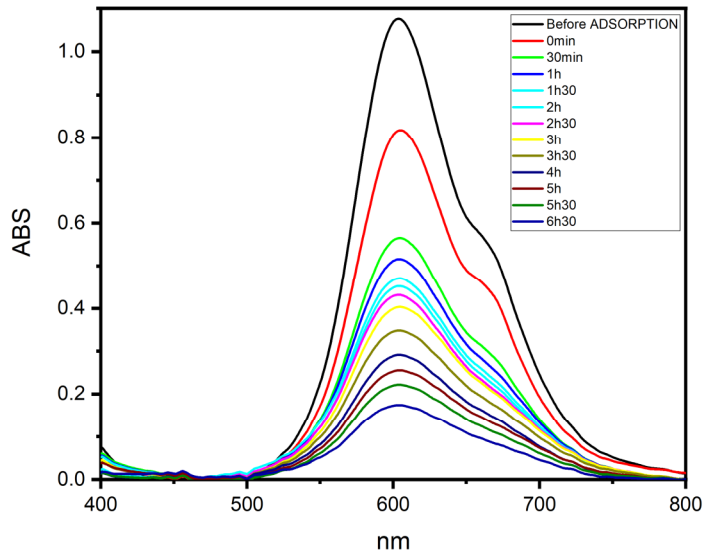

Figure 15: Evolution of Direct Blue 199 degradation under optimal conditions (pH=8, [TiO_2] = 1369.29 mg.L^{-1}, [H_2O_2] = 40 mmol.L^{-1}).

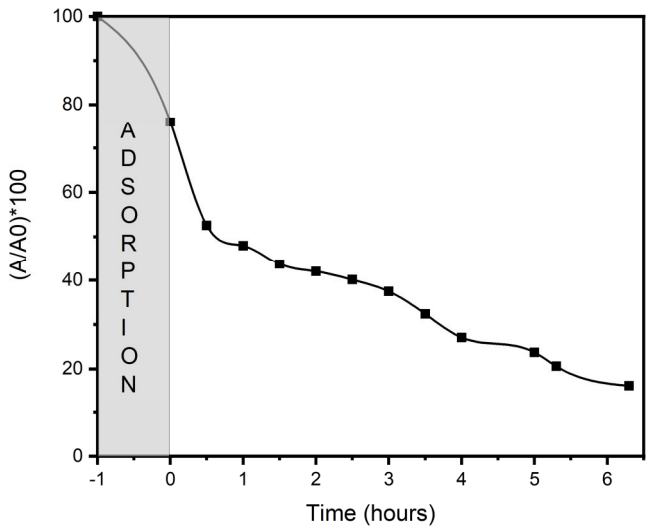

Figure 16: Photocatalytic activity of TiO_2 under optimal conditions (pH= 8, [TiO_2] = 1369.29 mg.L^{-1}, [H_2O_2] = 40 mmol.L^{-1}).

3.2.5. Kinetics study

These results allowed us to study the photodegradation reaction kinetics based on a pseudo-first-order equation, according to the Langmuir-Hinshelwood model ($-dC/dt = K_{app} \times C$), where C is the instantaneous concentration of the dye at time t, and K_{app} is the apparent first-order rate constant.

The kinetic data obtained in our study was well adapted to first-order pseudo kinetics. The K_{app} value was determined from the plot of $-\ln(C/C_0)$ as a function of t (Figure 17) and is well consistent with the literature for the photodegradation of organic compounds (Table 7) [28, 49-51].

A comparison with the work of Madhvi et al. [49], which have used titanium dioxide to degrade Direct Blue 199 dye. In their study, they were able to degrade up to 99% of the pollutant. The drawback is that they used capillary tubes with a diameter of one millimeter and a length of one meter and syringes to inject the polluted solution. The importance of our work, on one hand, is the use of commercial semiconductor without any previous or retrospective treatment. On the other hand, our semiconductor immobilization phase uses a low-cost technique that occurs at room temperature and does not require any other products apart from the

Table 7: K_{app} values for different wastewater photodegradation systems.

Photocatalysts	Light	contaminant	Initial concentration (ppm)	K_{app} (min^{-1})	Ref.
Titania/Gum Tragacanthin	UV(9W)	Methylene Blue	18.74	8×10^{-2}	[28]
TiO_2	Sun	Direct Blue 199	50 – 300	2.79×10^{-2}	[49]
$Ti_{0.95}Fe_{0.05}O_2$	UV-C 253.7 nm	Direct Blue 199	50	8.4×10^{-2}	[50]
$Ti_{0.96}Fe_{0.04}O_2$	UV	Direct Blue 199	50	6.2×10^{-2}	[51]

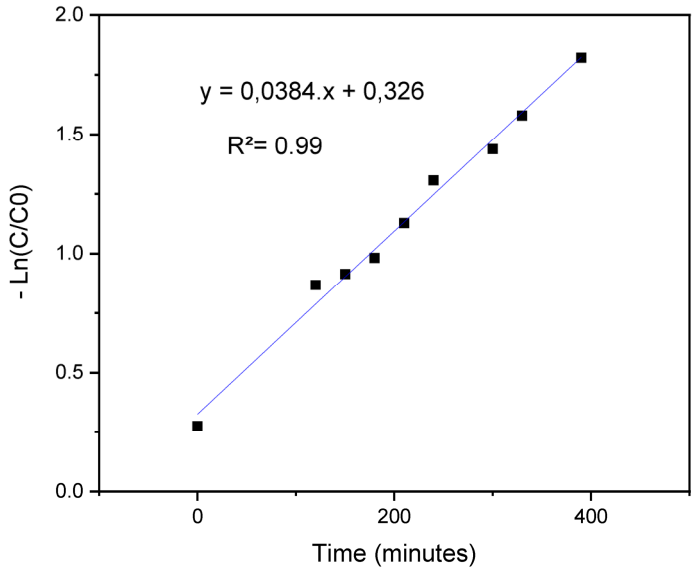

Figure 17: Kinetic study of dye degradation of Direct Blue 199 solution with TiO_2.

carrier polymer, which makes our method easy to use on a large scale. The works of Shu et al. [39, 52] showed another degradation technique to eliminate Direct Blue 199 and found difficulties degrading this dye. Even if they did not use semiconductors, their studies allowed us to choose the limits of hydrogen peroxide concentrations, which play a vital role in hydroxyl radical generation. Besides, the use of a low power UV-A lamp (9W) in our study allowed us to make a good comparison with theirs (they used several UV-C lights (253.7 nm) of which the least powerful was 70W). Furthermore, Saroj et al. [50, 51], obtained up to 98% degradation of Direct Blue 199 dye in only one hour treatment in a UV-C (<280nm) photoreactor lamp, and 3 h treatment in a tank under direct exposure to sun rays.

These results left us perplexed. Firstly, the high rate of degradation which we thought was due to the use of the mighty lamp. Except that, we noticed that they did not specify the initial operating conditions, and especially the pH of the medium; thus, the quantity of photocatalyst used was not evoked, which seems aberrant since we are on the point of studying its effect. Secondly, the use of a photocatalyst should not be detached from a surface charge study, which they did not carry out. What seems also strange is the lack of a reaction initiator, such as H_2O_2, known to be one of the most important factors [53]. Besides, the temperature of the medium was 44.5 °C, which seems very high and can alone cause the degradation of organic compounds [54].

Finally, the use of films with a TiO_2 mass percentage of no more than 14% has taught us, trough Experiment design, that it is necessary to look for the optimum conditions in pH and $[H_2O_2]$, where the minimum amount of semiconductor must is used. Operating conditions of pH= 8 and $[H_2O_2]$ = 40 $mmol.L^{-1}$ gave the best results with the desirability of 0.904. photocatalytic activity of our films on Direct Blue 199 dye is much lower than that on Methylene

blue observed in our previous work [12]. This is due to the size difference of the two molecules, and a possible formation of copper oxide by the copper element in the Direct Blue 199 molecule [51].

Even, the presence of a small agglomerated quantity of photocatalyst (<14%) contributes to the activity decrease [48]. Except that, a very apparent adsorption capacity was observed on the Direct Blue 199. These results can be explained by the appearance of pores, which increase due to the preparation technique inspired by the reverse-phase method, which is frequently used to design membranes [55] and favors this increase in porosity [56].

Finally, we note that our films have the advantage of being prepared under mild conditions and without any pretreatment. However, it requires a specific porosity optimization to limit and control the adsorption phenomena.

4. Conclusion

In summary, the photocatalytic activity of TiO_2 suspension deposited on PMMA polymer surface was studied for the degradation of Direct Blue 199 dye under UV irradiation. The design of experiment (DoE) was chosen to study and optimize the color degradation process. Based on the response surface methodology (RSM), a regression model was constructed and statistically validated. The developed model was used to predict the discoloring efficiency as a function of experimental factors. Finally, the following optimal conditions for efficient degradation of the dye were obtained: pH= 8, $[TiO_2]$ = 1369.29 $mg.L^{-1}$, $[H_2O_2]$ = 40 $mmol.L^{-1}$. Under these conditions, the maximum discoloring rate (R= 85%) was observed using UV irradiation. Besides, the prepared films have a high capacity to adsorb the dye in addition to the catalytic effect, which needs to be optimized during the preparation technique. We believe that our films have potential applicability in the field of dyestuffs.

5. References

1. P. Sirajudheen, S. Meenakshi, Facile synthesis of chitosan-La^{3+} graphite composite and its influence in photocatalytic degradation of methylene blue, *Int. J. Biol. Macromol.*, 133(2019), 253-261.
2. A. Khan, M. A. Aziz, M. Qamar, Simple and enhanced thermal immobilization of gold nanoparticles on TiO_2 coated ITO electrodes for photoelectrochemical water oxidation, *Chem. Sel.*, 2(2017), 7678-7683.
3. T. B. Veras, A. Luiz Ribeiro de Paiva, M. M. M. B. Duarte, D. C. Napoleão, J. J. da Silva Pereira Cabral, Analysis of the presence of anti-inflammatories drugs in surface water: A case study in Beberibe river-PE, Brazil., *Chemosphere*, 222(2019), 961-969.
4. M. O. Omorogie, A. E. Ofomaja, Clean technology and response surface approach for the photodegradation of selected antibiotics by catalyst supported on pine activated carbon, *Clean Technol. Environ. Policy*, 19(2017), 2191-2213.
5. J. He, Y. Zhang, Y. Guo, G. Rhodes, J. Yeom, H. Li, Photocatalytic degradation of cephalexin by ZnO nanowires under simulated sunlight : Kinetics, influencing factors, and mechanisms, *Environ. Int.*, 132(2019), 105-111.
6. S. Klementova, D. Kahoun, L. Doubkova, K. Frejlachova, M. Dusakova, M. Zlamal, Catalytic photodegradation of pharmaceuticals-homogeneous and heterogeneous photocatalysis, *Photochem. Photobiol. Sci.*, 16(2017), 67-71.
7. B. Vakili, B. Shahmoradi, A. Maleki, M. Safari, J. Yang, R. R. Pawar, Lee, Synthesis of immobilized cerium doped ZnO nanoparticles through the mild hydrothermal approach and their application in the photodegradation of synthetic wastewater, *J. Mol. Liq.*, 280(2019), 230-237.
8. A. J. Jafari, R. R. Kalantari, M. Kermani, M. H. Firooz, Photocatalytic oxidation of benzene by ZnO coated on glass plates under simulated sunlight, *Chem. Pap.*, 73(2019), 635-644.
9. M. Ait Himi, S. El Ghachtouli, A. Amarray, Z. Zaroual, P. Bonnaillie, M. Azzi, Removal of azo dye Calcon using polyaniline films electrodeposited on SnO_2 substrate, *Phys. Chem. Res.*, 8(2020), 111-124.
10. S. N. B. Saiful Amran, V. Wongso, N. S. Abdul Halim, M. K. Husni, N. S. Sambudi, M. D. H. Wirzal, Immobilized carbon-doped TiO_2 in polyamide fibers for the degradation of methylene blue, *J. Asian Ceram. Soc.*, 7(2019), 321-330.
11. Y. Lin, C. Weng, F. Chen, Key operating parameters affecting photocatalytic activity of visible-light-induced C-doped TiO_2 catalyst for ethylene oxidation, *Chem. Eng. J.*, 248(2014), 175-183.
12. O. Ounas, A. A. El Foulani, B. Lekhlif, J. Jamal-Eddine, Immobilization of TiO_2 into a poly methyl methacrylate (PMMA) as hybrid film for photocatalytic degradation of methylene blue, *Mater.*

Today Proc., 22(2020), 35-40.
13. S. M. Hashemi, K. Badii, S. Abdolreza, Study of immobilization of nano-TiO_2 for environmental aspects on glass by different resin families, *Prog. Color. Colorants Coat.*, 4(2010), 1-6.
14. S. K. Kassahun, Z. Kiflie, D. W. Shin, S. S. Park, W. Y. Jung, Y. R. Chung, Facile low temperature immobilization of N-doped TiO_2 prepared by sol–gel method, *J. Sol-Gel Sci. Technol.*, 83(2017), 698-707.
15. M. H. Alhaji, K. Sanaullah, A. Khan, A. Hamza, A. Muhammad, M. S. Ishola, A. R. H. Rigit, S. A. Bhawani, Recent developments in immobilizing titanium dioxide on supports for degradation of organic pollutants in wastewater- A review, *Int. J. Environ. Sci. Technol.*, 14(2017), 2039-2052.
16. K. (Guy) Vibulyaseak, S. (Benz) Deepracha, M. Ogawa, Immobilization of titanium dioxide in mesoporous silicas: Structural design and characterization, *J. Solid State Chem.*, 270(2019), 162-172.
17. A. M. A. Inamuddin, Gaurav Sharma, Amit Kumar, Eric Lichtfouse, *Nanophotocatalysis and Environmental Applications*, Springer, Cham, Switzerland, 2019, 49-82.
18. N. Becheikh, Modélisation et simulation numérique de la dégradation photocatalytique d'un polluant modèle dans un microréacteur, PhD thesis, Lorraine university, France, 2012.
19. S. Teixeira, H. Mora, L. M. Blasse, P. M. Martins, S. A. C. Carabineiro, S. Lanceros-Méndez, K. Kühn, G. Cuniberti, Photocatalytic degradation of recalcitrant micropollutants by reusable $Fe_3O_4/SiO_2/TiO_2$ particles, *J. Photochem. Photobiol. A Chem.*, 345(2017), 27-35.
20. A. H. Jawad, A. F. M. Alkarkhi, N. S. A. Mubarak, Photocatalytic decolorization of methylene blue by an immobilized TiO_2 film under visible light irradiation: optimization using response surface methodology (RSM), *Desalin. Water Treat.*, 56(2015), 161-172.
21. V. A. Sakkas, M. A. Islam, C. Stalikas, T. A. Albanis, Photocatalytic degradation using design of experiments: A review and example of the Congo red degradation, *J. Hazard. Mater.*, 175(2010), 33-44.
22. P. Pascariu, C. Cojocaru, N. Olaru, A. Airinei, Photocatalytic activity of ZnO–SnO_2 ceramic nanofibers for RhB Dye degradation: Experimental design, modeling, and process optimization, *Phys. Status Solidi Basic Res.*, 256(2019), 1-8.
23. R. Leardi, Experimental design in chemistry: A tutorial, *Anal. Chim. Acta*, 652(2009), 161-172.
24. P. Chawla, S. K. Sharma, A. P. Toor, Optimization and modeling of UV-TiO_2 mediated photocatalytic degradation of golden yellow dye through response surface methodology, *Chem. Eng. Commun.*, 206(2019), 1123-1138.
25. A. Zuorro, M. Fidaleo, R. Lavecchia, Response surface methodology (RSM) analysis of photodegradation of sulfonated diazo dye Reactive Green 19 by UV/H_2O_2 process, *J. Environ. Manage.*, 127(2013), 28-35.
26. C. Xu, G. P. Rangaiah, X. S. Zhao, Photocatalytic degradation of methylene blue by titanium dioxide: Experimental and modeling study, *Ind. Eng. Chem. Res.*, 53(2014), 14641-14649.
27. A. Toolabi, M. Malakootian, M. T. Ghaneian, A. Esrafili, M. H. Ehrampoush, M. AskarShahi, M. Tabatabaei, M. Khatami, Optimizing the photocatalytic process of removing diazinon pesticide from aqueous solutions and effluent toxicity assessment via a response surface methodology approach, *Rend. Lincei*, 30(2019), 155-165.
28. M. Rahimdokht, E. Pajootan, M. Ranjbar-Mohammadi, Titania/gum tragacanth nanohydrogel for methylene blue dye removal from textile wastewater using response surface methodology, *Polym. Int.*, 68(2019), 134-140.
29. P. W. Koh, L. Yuliati, S. L. Lee, Kinetics and optimization studies of photocatalytic degradation of methylene blue over Cr-doped TiO_2 using response surface methodology, *Iran. J. Sci. Technol. Trans. A Sci.*, 43(2019), 95-103.
30. H. Eskandarloo, A. Badiei, M. A. Behnajady, Application of response surface methodology for optimization of operational variables in photodegradation of phenazopyridine drug using TiO_2/CeO_2 hybrid nanoparticles, *Desalin. Water Treat.*, 54(2015), 3300-3310.
31. S. Nur, S. Jefri, A. Halim, E. Noryana, Asian journal of green chemistry orginal research article response surface methodology : photodegradation of methyl orange by CuO/ZnO under UV light irradiation, *Asian J. Green Chem.*, 3(2019), 271-287.
32. A. H. Abdullah, H. J. M. Moey, N. A. Yusof, Response surface methodology analysis of the photocatalytic removal of Methylene Blue using bismuth vanadate prepared via polyol route, *J. Environ. Sci. (China)*, 24(2012), 1694-1701.
33. S. Baghbani Ghatar, S. Allahyari, N. Rahemi, M. Tasbihi, Response surface methodology optimization for photodegradation of methylene blue in a ZnO coated flat plate continuous photoreactor, *Int. J. Chem. React. Eng.*, 16(2018), 1-14.
34. I. H. Cho, K. D. Zoh, Photocatalytic degradation of azo dye (Reactive Red 120) in TiO_2/UV system: Optimization and modeling using a response surface methodology (RSM) based on the central composite design, *Dye. Pigment.*, 75(2007), 533-543.
35. A. Mehrizad, P. Gharbani, Removal of methylene blue from aqueous solution using nano-TiO_2/UV Process: optimization by response surface methodology, *Prog. Color Colorants Coat*, 9(2016), 135-143.
36. T. K. M. Prashantha Kumar, T. R. Mandlimath, P. Sangeetha, P. Sakthivel, S. K. Revathi, S. K. Ashok Kumar, S. K. Sahoo, Highly efficient performance of activated carbon impregnated with Ag, ZnO and Ag/ZnO nanoparticles as antimicrobial materials, *RSC Adv.*, 5(2015), 108034-108043.

37. P. Calza, V. A. Sakkas, C. Medana, C. Baiocchi, A. Dimou, E. Pelizzetti, T. Albanis, Photocatalytic degradation study of diclofenac over aqueous TiO_2 suspensions, *Appl. Catal. B Environ.*, 67(2006), 197-205.
38. M. Haji Alhaji, K. Sanaullah, S. Fong Lim, A. Ragai Henry Rigit, A. Hamza, A. Khan, Modeling and optimization of photocatalytic treatment of pre-treated palm oil mill effluent (POME) in a UV/TiO_2 system using response surface methodology (RSM), *Cogent Eng.*, 4(2017), 1-17.
39. H. Y. Shu, M. C. Chang, Decolorization and mineralization of a phthalocyanine dye C.I. Direct Blue 199 using UV/H_2O_2 process, *J. Hazard. Mater.*, 125(2005), 96-101.
40. O. Ounas, B. Lekhlif, J. Jamal-eddine, The facile immobilization of ZnO into a polymer surface for photodegradation of organic contaminants, *Mater. Today Proc.*, 23(2020).
41. S. Sugumaran, C. S. Bellan, Transparent nano composite PVA-TiO_2 and PMMA-TiO_2 thin films: Optical and dielectric properties, *Optik (Stuttg).*, 125(2014), 5128-5133.
42. P. Srinivasu, S. P. Singh, A. Islam, L. Han, Novel approach for the synthesis of nanocrystalline anatase titania and their photovoltaic application, *Adv. Optoelectron.*, 2011(2011), 47-59.
43. A. Di Mauro, M. Cantarella, G. Nicotra, G. Pellegrino, A. Gulino, M. V. Brundo, V. Privitera, G. Impellizzeri, Novel synthesis of ZnO / PMMA nanocomposites for photocatalytic applications, *Nat. Publ. Gr.*, 33(2017), 1-12.
44. P. Bindu, S. Thomas, Estimation of lattice strain in ZnO nanoparticles: X-ray peak profile analysis, *J. Theor. Appl. Phys.*, 8(2014), 123-134.
45. S. Hammani, A. Barhoum, M. Bechelany, Fabrication of PMMA/ZnO nanocomposite: effect of high nanoparticles loading on the optical and thermal properties, *J. Mater. Sci.*, 53(2018), 1911-1921.
46. Z. Adlan, M. Hir, P. Moradihamedani, A. H. Abdullah, M. A. Mohamed, Immobilization of TiO_2 into polyethersulfone matrix as hybrid film photocatalyst for effective degradation of methyl orange dye, *Mater. Sci. Semicond. Process.*, 57(2017), 157-165.
47. C. A. Schneider, W. S. Rasband, K. W. Eliceiri, NIH Image to ImageJ: 25 years of image analysis, *Nat. Methods*, 9(2012), 671-675.
48. D. Jassby, J. Farner Budarz, M. Wiesner, Impact of aggregate size and structure on the photocatalytic properties of TiO_2 and ZnO nanoparticles, *Environ. Sci. Technol.*, 46(2012), 6934-6941.
49. Madhvi, L. Singh, S. Saroj, Y. Lee, S. V. Singh, Facile synthesis of nano-crystalline anatase TiO_2 and their applications in degradation of Direct blue 199, *J. Mater. Sci. Mater. Electron.*, 27(2016), 2581-2588.
50. S. Saroj, L. Singh, R. Ranjan, S. V. Singh, Enhancement of photocatalytic activity and regeneration of Fe-doped TiO_2 ($Ti_{1-x}Fe_xO_2$) nanocrystalline particles synthesized using inexpensive TiO_2 precursor, *Res. Chem. Intermed.*, 45(2019), 1883-1906.
51. S. Saroj, L. Singh, S. V. Singh, Photodegradation of Direct Blue-199 in carpet industry wastewater using iron-doped TiO_2 nanoparticles and regenerated photocatalyst, *Int. J. Chem. Kinet.*, 51(2019), 189-205.
52. H. Y. Shu, Degradation of dyehouse effluent containing C.I. Direct Blue 199 by processes of ozonation, UV/H_2O_2 and in sequence of ozonation with UV/H_2O_2, *J. Hazard. Mater.*, 133(2006), 92-98.
53. O. Prieto, J. Fermoso, Y. Nuñez, J. L. Del Valle, R. Irusta, Decolouration of textile dyes in wastewaters by photocatalysis with TiO_2, in *Solar Energy*, 79(2005), 376-383.
54. S. Z. Zhang, X. G. Luo, X. Y. Lin, Thermocatalytic degradation of methylene blue using negative temperature coefficient resistor, *Adv. Mater. Res.*, 726–731(2013), 2036-2039.
55. Y. Chaouqi, R. Ouchn, I. Touarssi, I. Mourtah, M. El Bouchti, L. Lebrun, O. Cherkaoui, M. Hlaibi, Polymer inclusion membranes for selective extraction and recovery of hexavalent chromium ions from mixtures containing industrial blue P3R dye, *Ind. Eng. Chem. Res.*, 58(2019), 18798-18809.
56. O. Benhabiles, F. Galiano, T. Marino, H. Mahmoudi, H. Lounici, A. Figoli, Preparation and characterization of TiO_2 -PVDF/PMMA blend membranes using an alternative non-toxic solvent for UF/MF and photocatalytic application, *Molecules*, 24(2019), 1-20.

How to cite this article:
O. Ounas, B. Lekhlif, J. Jamal-Eddine, Effect of Three Operating Variables on Degradation of Direct Blue 199 by TiO_2 Immobilized into a Polymer surface: Response Surface Methodology., *Prog. Color Colorants Coat.*, 14 (2021), 161-178.